Improving Wireless Power Transfer Efficiency Using Hollow Windings With Track-Width-Ratio

Samuel R. Cove, *Member, IEEE*, Martin Ordonez, *Member, IEEE*, Navid Shafiei, *Student Member, IEEE*, and Jianglin Zhu, *Student Member, IEEE*

***Abstract*—With the widespread growth of slim portable electronics, research into planar spiral windings for wireless power transfer (WPT) battery charging systems has gained a lot of attention due to their low profile, reproducibility, and manufacturability. The major design goal for windings in WPT systems is high-quality factor (Q) for a given inductance. This study presents a new method to improve Q by using a nonunity track-width-ratio (TWR) geometrical arrangement in conjunction with increasing the inner radius of winding to make an improved hollow planar spiral winding. The inductance regulation of this technique combined with its exceptional improvements in Q make it a superior choice for resonant WPT systems. Inductance and resistance models are provided in order to assess the Q improvement. A 5-W, 110–200-kHz WPT system was built and tested based on the wireless power consortium Qi standard to confirm the advantages of the improved windings on the transmission efficiency of the system. An increase from 70% to 90% are observed from employing the proposed winding technique designed using the provided models.**

NOMENCLATURE

$\Phi_{\text{cond,rec}}, \Phi_{\text{prox,recprox}}$	Normalized conduction and proximity loss function for planar spiral windings.
a	Ratio of successive turn widths (TWR).
C_l	Clearance distance between turns.
d	Spacing between winding and shielding.
f	Frequency of operation.
f_r	Resonant frequency.
GMD	Geometric Mean Distance.
l	The distance over which power is transferred wirelessly.
l_j, l_k, l_{j+k}	Length of turn-segments j, k, and the vector sum of $j+k$.
L_N	The total self-inductance of the planar spiral winding.
M_{jk}	Mutual inductance between winding portions j and k.
M_N	Total mutual inductance of the planar spiral winding.
N	Number of turns.
N_L	Number of layers.
$R_{\text{cond}}, R_{\text{prox}}$	Conductive and proximity resistance components.
r_n, r_j, r_k	Radius of nth, jth, and kth winding turn.
s	Spacing between layers.
t	Conductor thickness.
W	Width of the outermost turn.
w_n, w_j, w_k	Width of the nth, jth, and kth winding turn.
x_i	Inner radius of a planar spiral winding.
x_o	Outer radius of a planar spiral winding.

Manuscript received April 6, 2015; accepted October 27, 2015. Date of publication November 6, 2015; date of current version March 25, 2016. Recommended for publication by Associate Editor M. Duffy.

S. R. Cove, M. Ordonez, and N. Shafiei are with Electrical and Computer Engineering, University of British Columbia, Vancouver V6T 1Z4, BC Canada (e-mail: srcove@ieee.org; mordonez@ieee.org; mr.navid.shafiei@ieee.org).

J. Zhu is currently with the Department of Electrical, Computer, and Energy Engineering, University of Colorado Boulder, Boulder, CO 80309-0425 USA (e-mail: jianglin.zhu@colorado.edu).

Color versions of one or more of the figures in this paper are available online at http://ieeexplore.ieee.org.

Digital Object Identifier 10.1109/TPEL.2015.2498638

I. INTRODUCTION

RECENT advancements in wireless power technology for slim consumer electronics are providing an opportunity for the use of planar spiral windings as transmitting and receiving windings [1]–[6]. Their low profile and weight, combined with high repeatability and reproducibility make them ideal candidates for this task. However, maximizing the performance of the winding is a complex design task, as there are an excessive number of ways to modify the winding layout, all of which play important roles in the quality of the winding.

For a resonant wireless power transfer (WPT) winding of a constant separation, the highest importance is to improve its quality factor (Q) [7]–[13], since the losses are heavily caused by the high-frequency winding resistance. There has been interesting research into methods to order to improve the design of planar spiral windings [14]–[20]. A method of improving the performance of circular planar spirals through removing the inner turns to create a hollow spiral has been proposed [14], [15] and is highlighted in Fig. 1(b). A resistance calculation method for circular and rectangular spiral windings with varying track widths has also been presented [16]. Preliminary study has been completed on characterizing parasitic effects for specific spiral geometries for interlocking-square [17] and circular [18] spiral windings for planar transformers. Track width variations have also been demonstrated to improve the Q of square integrated inductors for radio frequency applications [19], [20] for square spirals. These important contributions improve the quality factor of the planar spiral windings, but the hollow spiral windings suffer from a reduction in inductance by about 10–15% in order to hit max Q [15]. The tactic of varying trace widths reduces the overall resistance of the winding, but by itself it still retains turns in the center of the spiral which exhibit high eddy current losses induced by the strong central magnetic field.

Previous study has aimed to model the effect of high-frequency winding resistance and losses in planar spirals [21]–[24]. A 1-D model provided an approximation for wire-wound magnetics [21], which was later improved to include edge effects with a series of 2-D models for rectangular [22]

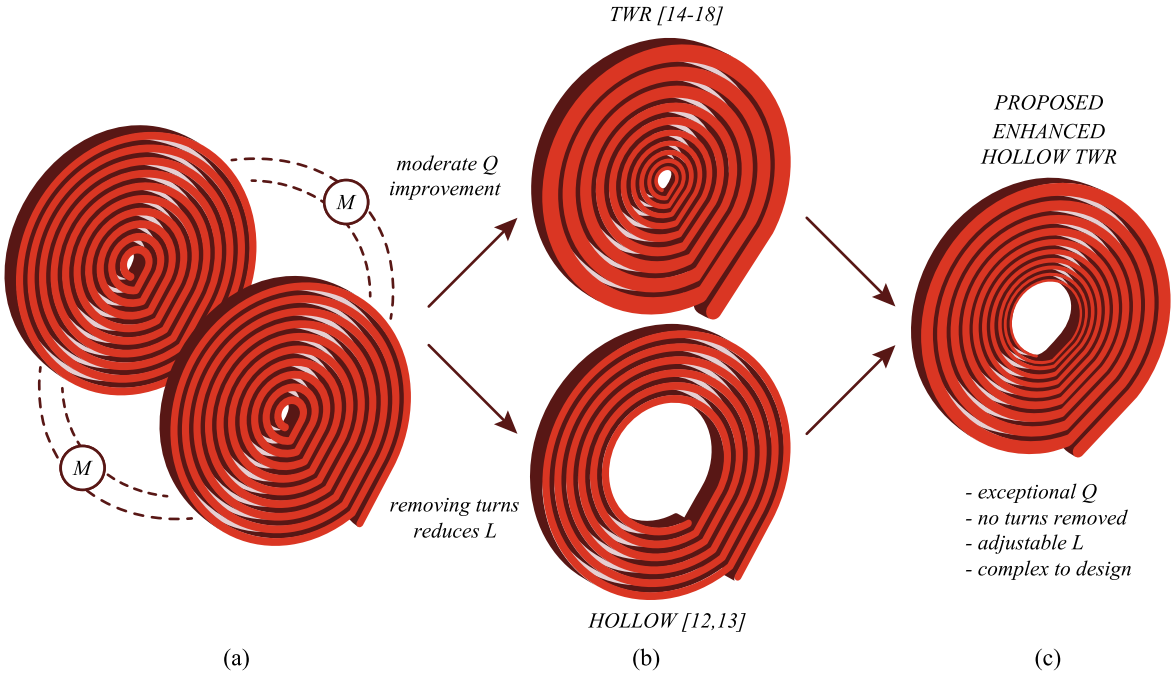

Fig. 1. Circular planar spiral windings: (a) baseline full winding employed in WPT (b) two upgrade paths previously presented for the baseline case (TWR and hollowing by removing turns) (c) proposed hollow spiral winding with an increased inner radius and a nonunity TWR between turns.

and arbitrary [23] cross-section conductors. This study was later expanded to include concentric planar spiral windings by employing a model based on finite-element analysis (FEA) [24]. These studies have expanded the ability to predict the behavior of traditional planar and wire-wound windings, but the tools are not readily available to observe the effect of advanced winding techniques such as employing a variety of track widths within one winding.

The proposed technique to improve the performance of planar spiral windings is a significant enhancement of the hollow approach combined with varying track widths as illustrated in Fig. 1(c). Instead of removing turns, this technique expands the inner radius of the winding while keeping the number of turns constant in order to avoid high-frequency losses on the interior turns without compromising inductance. The second step is to apply a constant track-width-ratio (TWR) which reduces the width of turns as they move towards the center of the winding with a constant ratio. This reduces the resistance of the winding further, creating a winding with an exceptional Q value. This combined technique significantly improves the Q value higher than removing turns or applying TWR independently, and when properly tuned it does not reduce the inductance of the winding. The latter requirement is important for resonant WPT systems in which there are strict requirements on the inductance in order to achieve resonance with a static-value series or parallel capacitor.

While this technique dramatically improves the Q value of planar windings, it increases the complexity of the windings arrangement over employing TWR or hollow windings individually. In order to model the improvements of this technique, an inductance model is derived from the work of Grover [25] and Greenhouse [26]. The self and mutual inductances are modeled and combined to determine the overall inductance of the winding structure. The ac-resistance model is a modification of a semianalytical approach to planar spiral winding resistance first proposed in [24]. The results from the inductance and resistance are used to determine the Q of the resultant winding. The results are compared to experimentally manufactured windings for all techniques represented in Fig. 1, including the proposed combination of a hollow winding with TWR. The resultant inductance, quality factor, and thus, resistance are presented in conjunction with the performance when employed in a 5-W, 110–205-kHz WPT system. Transfer efficiencies upward of 90% have been attained with the proposed windings under similar conditions to a Qi wireless power standard, an increase from the 70% observed for the baseline case described in Fig. 1(a) and 80% for the traditional hollow winding in Fig. 1(b).

This study contributes to the spiral design for WPT systems by:

1) providing the modeling tools for the inductance and ac resistance of changing track widths in hollow planar spiral windings;
2) addressing the high ac losses in the center of planar spiral windings to improve the efficiency for resonant WPT systems;
3) providing a superior technical solution to improve the Q of the transmission windings in WPT systems without the drawback of reduced inductance;
4) confirming the exceptional performance of the proposed technique through a 5-W, 110–200-kHz resonant WPT system.

Predicting the performance of the proposed windings is more complex than traditional winding design, but much higher quality factors can be achieved, no turns are removed, and the inductance can be tuned to the value required for resonance. This is a significant improvement over previous approaches to planar spiral winding design.

II. Hollow Planar Spiral Winding With TWR

Planar spiral windings suffer from high ac losses due to high magnetic field strength normal to their surface, creating

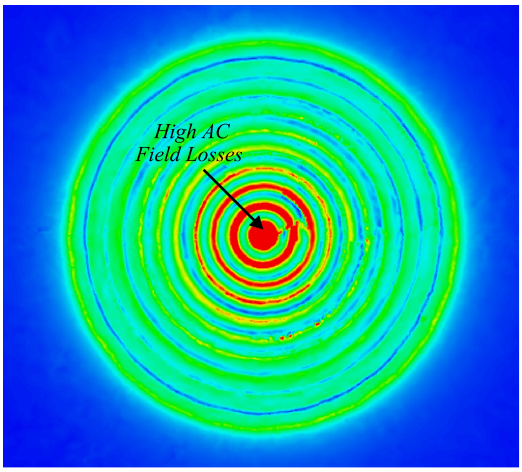

Fig. 2. Magnitude of the magnetic field strength, H, for a horizontal cross section of a circular planar spiral winding.

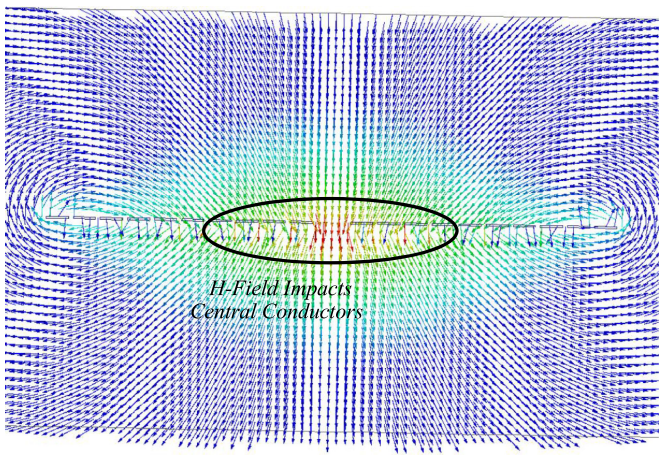

Fig. 3. Magnetic field intensity vector, $\vec{H}$, for a vertical cross section of a circular planar spiral winding.

high-frequency eddy-current losses. This is particularly concerning in the center of concentric planar spiral windings where the magnetic field strength is at its highest. Figs. 2 and 3 contain the magnitude and vector representations of the magnetic field around a circular planar spiral winding. The additive nature of the field in the center of the winding creates an area in which high eddy-current losses are created within the inner turns.

Fig. 4 provides a diagram of the proposed winding to avoid the high losses in the center of the spiral while not compromising inductance. The spiral has a constant thickness (t), a moderate ratio of inner radius (x_i) to outer radius (x_o), a small clearance between traces (C_l), and most importantly a nonunity ratio of track widths between each turn (a) defined as the TWR. N is the number of turns and W is defined as the width of the outer turn. The width of any individual turn (w_n) is given by

$$w_n = a^{n-1}W \tag{1}$$

where n represents the turn number, starting from the outer turn, ranging from 1 to N. Fig. 4(a) shows an isometric view view of the windings while Fig. 4(b) highlights a cross section of the

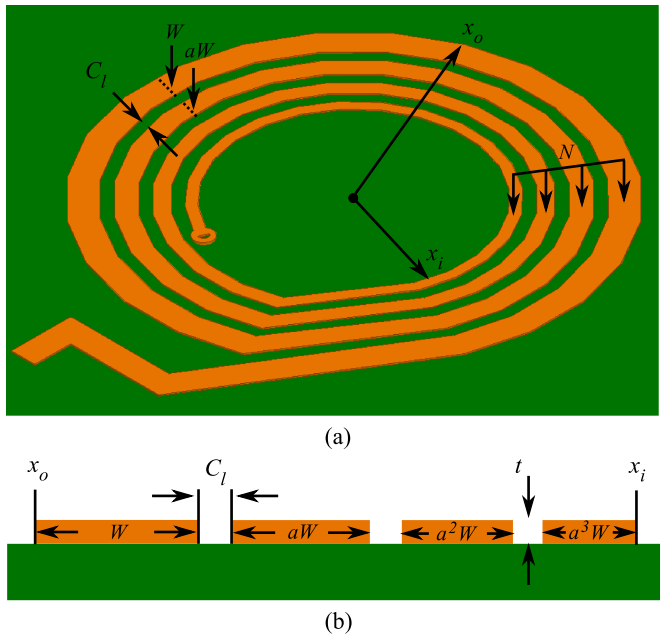

Fig. 4. Circular planar spiral winding with TWR applied, indicating the important spiral dimensions (a) isometric view (b) zoomed-in vertical cross section.

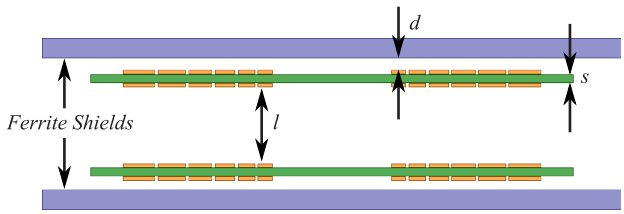

Fig. 5. Shielded WPT setup employing circular planar spiral windings with TWR employed, indicating important dimensions with regards to winding and shielding placement.

winding, where the ratio between the widths of adjacent turns is magnified. This study investigates purely the case where $a < 1$, such that the conductor widths decrease as the turns progress to the center of the winding, leaving less conductor for the high magnetic fields to penetrate, thus, reducing high-frequency resistive losses.

Each turn of the circular spiral winding with nonunity TWR is comprised of an approximately 330° circular arc which uses straight conductors to seamlessly transition between turns of unequal track width. This is emphasized in Fig. 4(a). Compared to an ideal spiral, the overall conductor length of the proposed design deviates by less than 2%, ensuring the turn-connections do not hinder the performance.

An added benefit for this technique, when employed in a WPT system, is that the center of the winding spiral can now be used to place a magnet, which is one way in which transmission and receiving windings can be aligned [27]. Fig. 5 depicts two of the proposed hollow planar spiral windings with TWR being employed in a low-power WPT system. The number of layers in each winding (N_L) is two in this case, each employing the same nonunity TWR. The windings are sandwiched between two ferrite plates which provide the necessary magnetic shielding for the system while helping to improve the coupling. The distance over which power is transferred is l, the gap between

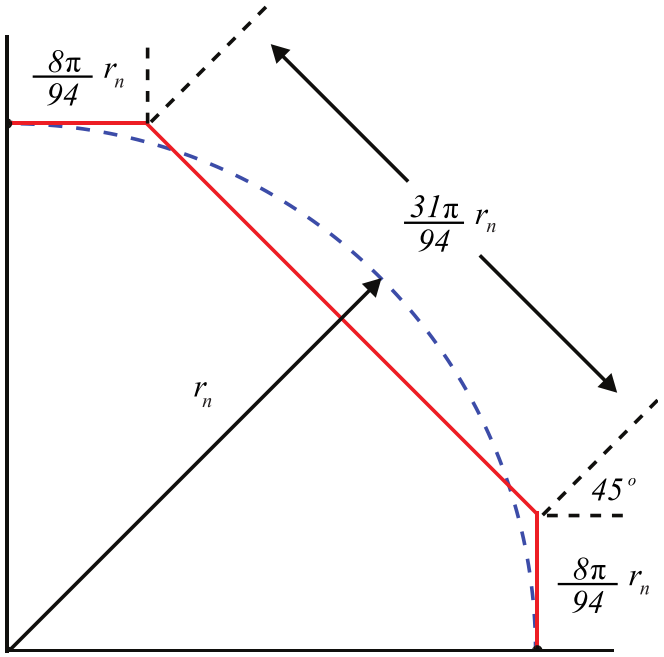

Fig. 6. Schematic highlighting the relationship between the length of an octagonal corner (red) and the radius of a racetrack approximation (blue) for the nth turn of an N turn winding.

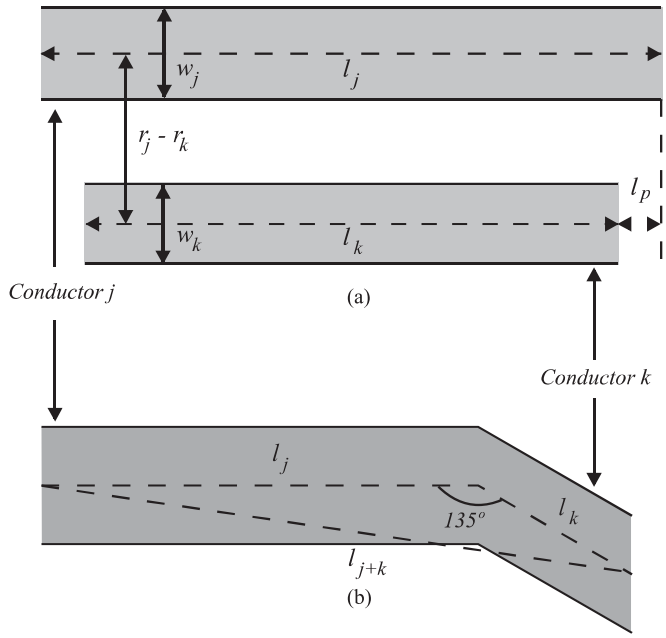

Fig. 7. Two important cases for mutual inductance calculations with important dimensions: (a) two parallel conductors of uneven length and width centered on a vertical axis (b) two uneven length conductors of even width connected at one end subtending an angle of 135°.

the winding and the shielding is d, and the interlayer spacing is s.

III. Quality Factor Modeling for Hollow Windings With TWR

The quality factor of a winding is defined by the relation

$$Q = \frac{\omega L}{R} \tag{2}$$

so to establish the fundamentals of this approach, the inductance and resistance of the hollow winding structure with TWR applied are investigated.

A. Inductance Modeling

The inductance of the structure is derived from the work of Grover and Greenhouse [25], [26], where the self-inductance is calculated by each piece of the winding and combined with the mutual inductance of each pair of winding segments to determine the overall inductance. The simplification that is made in this study is that the winding is considered to be composed of fully concentric circular turns with no interconnections, and each 90° arc is approximated by three straight winding sections as established in Fig. 6. In this way, the total length of the nth turn, l_n, stays the same at

$$l_n = 2\pi r_n \tag{3}$$

where r_n is the radius of the center of the circular turn, which can be established from the following relation:

$$r_n = x_i + (n-1)C_l + \frac{a^{N-n}}{2}W + \sum_{k=1}^{n-1} a^{N-k}W \tag{4}$$

where $n = 1$ indicates the innermost turn and N is the outermost turn. Applying the work of Grover and Greenhouse, the resultant self-inductance of the structure is

$$L_{s_N}(\mu\text{H}) = \sum_{n=1}^{N} 0.002 l_n \left[\log_e\left(\frac{2l_n}{t + a^{N-n}W}\right) + 0.50049 + \left(\frac{t + a^{N-n}W}{3l_n}\right)\right] \tag{5}$$

where W is the width of the widest conductor, which is defined by

$$W = (x_o - x_i - (N-1)C_l)\frac{(1-a)}{1-a^N}. \tag{6}$$

After the self-inductance is established, the mutual inductance must be calculated, with some simplifications. First, the same simplification from Fig. 6 is employed such that all arcs are turned to straight paths, and a further simplification is that the mutual inductance is only significant if the conductors are parallel with different lengths and widths [highlighted in Fig. 7(a)], or connected at a 135° angle with different lengths [highlighted in Fig. 7(b)]. All perpendicular conductors are considered to have no contribution to the mutual inductance, and the geometric mean distance (GMD) between any parallel conductors is considered to be the distance between their centers. Important distances and conductor lengths are labeled in Fig. 7.

The mutual inductance contribution of the parallel planar conductors from Fig. 7(a) is first calculated as if they had the same length, l

$$M_l(\mu\text{H}) = 2l\left[\log_e\left\{\frac{l}{\text{GMD}} + \left(1 + \frac{l^2}{\text{GMD}^2}\right)^{\frac{1}{2}}\right\} - \left(1 + \frac{\text{GMD}^2}{l^2}\right)^{\frac{1}{2}} + \frac{\text{GMD}}{l}\right] \tag{7}$$

where l is the length of the conductors and GMD is the geometric mean distance between the two conductors. The GMD for our case is assumed to be the distance between the centers of the two parallel conductors, which is conveniently the difference between the turns' original radii

$$\text{GMD} = r_j - r_k \tag{8}$$

which can be calculated from (4). In order to correct the value for the fact that the conductors are actually uneven in length, the mutual inductance (M_{jk}) is corrected in the following way:

$$M_{\text{jk}} = M_{k+p} - M_p \tag{9}$$

where M_{k+p} is the mutual inductance calculated in (7) for $l = l_k + l_p$ and M_p is the same with $l = l_p$. Both cases employ (8).

The mutual inductance contribution from the conductors demonstrated in Fig. 7(b) are calculated using the following relation:

$$M_{\text{jk}}\,(\mu\text{H}) = 0.001\left(\frac{\sqrt{2}}{2}\right) l_j \left[\log_e \frac{1+\frac{l_k}{l_j}+\frac{l_{j+k}}{l_j}}{1-\frac{l_k}{l_j}+\frac{l_{j+k}}{l_j}} + \frac{l_k}{l_j}\log_e \frac{\frac{l_k}{l_j}+\frac{l_{j+k}}{l_j}+1}{\frac{l_k}{l_j}+\frac{l_{j+k}}{l_j}-1}\right] \tag{10}$$

where l_j and l_k are are functions of r_n

$$l_j = \frac{16\pi}{94} r_n \tag{11}$$

$$l_k = \frac{31\pi}{94} r_n \tag{12}$$

and l_{j+k} is highlighted in Fig. 7 and is calculated by employing the law of cosines as

$$l_{j+k}^2 = l_j^2 + l_k^2 - \sqrt{2} l_j l_k. \tag{13}$$

The overall mutual inductance (M_N) is the sum of the individual mutual inductances

$$M_N = \sum_{j \neq k} M_{\text{jk}}. \tag{14}$$

The parallel conductor components are positive for those whose currents are traveling in the same direction, and are negative for conductors whose currents are traveling in opposite directions. The total inductance (L_N) is the sum of the self and mutual inductances:

$$L_N = L_s + M_N. \tag{15}$$

The end result of applying TWR to planar spiral windings is highlighted in Fig. 8. As TWR is applied, the inductance decreases at an exponential rate which is dependent upon the number of turns employed.

B. AC Resistance Modeling

The ac resistance model of the hollow spiral winding with TWR employed is based on previous study on a quasi-analytical approach to high-frequency resistance estimation in planar spiral windings [24]. FEA was inserted into the analytical model in a normalized fashion based on the conductor width and thickness in terms of the skin depth. The losses were broken down into conduction losses and proximity losses. Since the proximity losses are induced by magnetic fields which impinge the conductors at various angles, there is an x and z component to the proximity loss term (where z is vertically upward). The models are duplicated here for clarity [24]

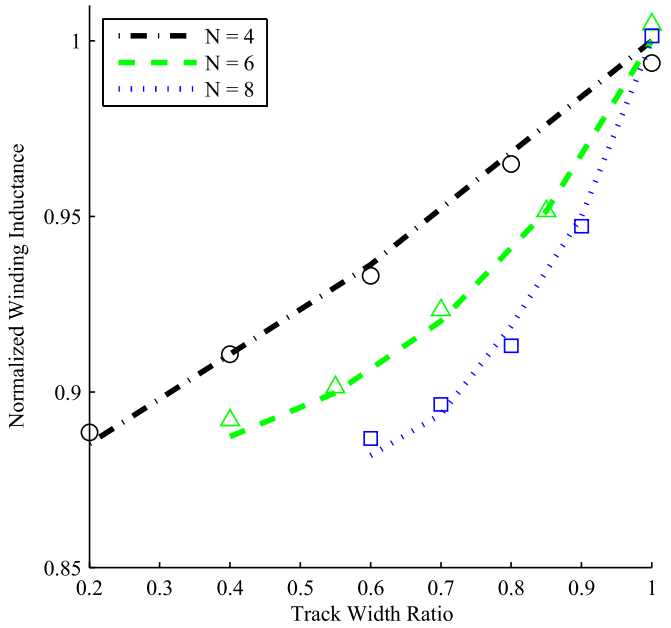

Fig. 8. Inductance trend of hollow planar spiral windings with TWR applied for various number of turns: predicted versus actual. Winding specs contained in Table I.

$$R_{\text{ac}} = R_{\text{cond}} + R_{\text{prox},x} + R_{\text{prox},z} \tag{16}$$

where

$$R_{\text{cond}} = \frac{1}{wt\sigma}\Phi_{\text{cond,rec}}\left(\frac{w}{\delta}, \frac{t}{\delta}\right) \tag{17}$$

$$R_{\text{prox},x} = \frac{1}{wt\sigma}\Phi_{\text{prox,rec}}\left(\frac{w}{\delta}, \frac{t}{\delta}\right)|\overline{H}_{o,x}|^2 \tag{18}$$

$$R_{\text{prox},z} = \frac{1}{wt\sigma}\Phi_{\text{prox,rec}}\left(\frac{w}{\delta}, \frac{t}{\delta}\right)|\overline{H}_{o,z}|^2. \tag{19}$$

Each resistance value is per unit length, and the Φ values are normalized frequency and geometry dependent values which are determined from FEA and are visually represented in [24]. The magnitudes of the orthogonal x and z components of the magnetic field from the proximity effect are estimated by the FEA as well.

These models were established for windings with a constant conductor width. In this study, further FEA was performed in order to establish the effect of a nonunity TWR for hollow planar spiral windings. The result is a quadratic function of resistance based on frequency and the previously defined physical characteristics of the winding, which is normalized to the resistance value, R_{ac} from (16). The resultant model of ac resistance of the hollow planar spiral winding with TWR is given by

$$\frac{R}{R_{\text{ac}}} = \left(\frac{NN_L x_i}{C_l f x_o}a^2 + \frac{N_L f x_o}{N x_i C_l}a + \frac{x_o^2\sqrt{f}C_l}{NN_L x_i}\right) \tag{20}$$

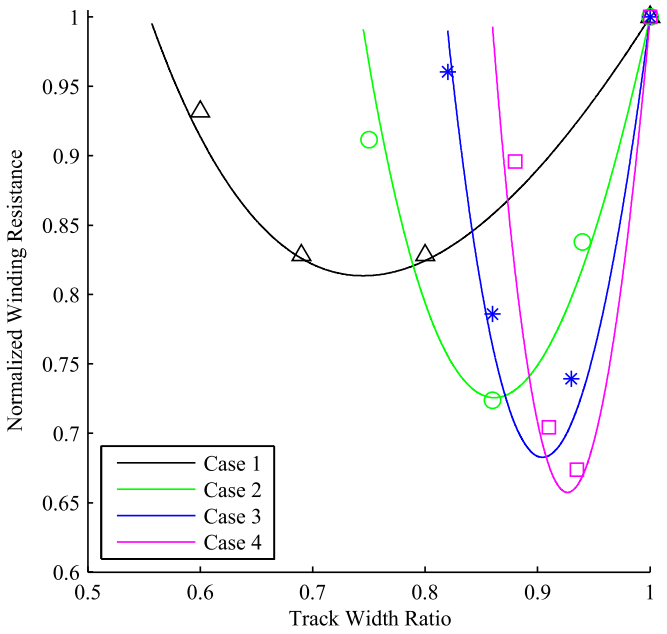

Fig. 9. Resistance trend of hollow planar spiral windings with TWR applied. Predicted values are compared to 16 experimental measurements. Case 1 is for $N = 2$, $f = 50$ kHz. Case 2 is $N = 2$, $f = 250$ kHz. Case 3 is for $N = 8$, $f = 50$ kHz. Case 2 is $N = 8$, $f = 250$ kHz. The rest of the dimensions follow those documented in Table I.

which is a parabola with no roots and a minimum that falls between $a = (0, 1)$. That minimum can be determined by differentiating (20) and setting the result equal to zero

$$0 = \left(\frac{2NN_L x_i}{C_l f x_o} a_{\min} + \frac{N_L f x_o}{N x_i C_l} \right). \tag{21}$$

The model is accurate over the interval $a = [2a_{\min} - 1,1]$, at which point the resistance of the winding exceeds R_{ac} and there is no benefit derived from employing TWR. Fig. 9 presents these curves for various combinations of turns and frequency. Some insights which can be gained from this plot are that $a_{\min}$ increases as the number of turns increase, and that the impact of a on resistance increases with the number of turns and the frequency of operation.

IV. Quality Factor Trends in Hollow Planar Spiral Windings With TWR

The models proposed in this study provide insight into the effect of changing the TWR on the inductance and resistance of planar spiral windings. This section extends this study by studying a subset of windings in order to confirm that the approach of applying TWR while increasing the internal radius can practically achieve a significant improvement in quality factor in WPT systems and provide some guidelines for the design of such windings.

The inductance and ac resistance of 50 windings with various x_i and a values were analyzed by employing the previously proposed models, while employing different numbers of layers and frequencies. The quality factor of each winding was then calculated using (2) and trends were determined through the application of regression analysis. This study was performed over the range of factors displayed in Table I in order to find a

TABLE I
Factors Range of Operation

Factor	Value	Units
x_i	1–5	mm
a	0.8–1.0	
N_L	2, 4	
f	100–500	kHz
N	10	turns
x_o	15	mm
C_l	0.25	mm
t	0.105	mm
d	0.5	mm
s	0.5	mm

winding which would conform to the electrical requirements of the Qi specification [27]. The resulting 3-D plots are presented in Fig. 10. It highlights that there is a maximum Q for a given footprint and frequency, for this case. The quality factor improves with an increase in a and x_i until a peak is reached, and then reduces. The peak Q can be significantly higher than the baseline winding, in this case an increase of 400% is observed. This is natural because of the way TWR reduces the resistance of the winding as demonstrated in Fig. 9. If this plot is observed in slices of constant inductance, from Fig. 10(a), it still exhibits this behavior for every slice. Fig. 10(d) demonstrates the changes in the surface when more layers are added. In this case, the peak Q is attained from higher values of x_i and a, at a value higher than the 400% observed in Fig. 10(b). This makes sense since the field is stronger in the middle with the added layers, requiring a higher internal radius and stronger TWR to reduce the high-frequency resistance. It is important to notice that the inductance does not reduce to provide this exceptional behavior. The following section confirms the models experimentally, while investigating the performance of the proposed windings compared to traditional hollow windings.

V. Experimental Verification

Fig. 12(a) shows a series of circular planar spiral windings that were manufactured in order to test the models developed in the previous section and their L, R, and Q were measured by employing a frequency response analyzer and later confirmed with a KT4990A impedance analyzer. Excellent correlation was found between the measurements and the calculated results from the models employed in this study, as can be observed in Fig. 11. Tight tolerances, less than 5%, are noticed between predicted and actual values for L, R, and Q. In this situation, they are normalized parameters, where L was normalized to 40 μH, R was normalized to 250 $m\Omega$, and Q was normalized to 25.

A. Low-Power WPT Application

The proposed hollow planar spiral windings with TWR have the benefits of greatly increased quality factor compared to traditional approaches and have the added benefit of being able to tune the inductance up or down without changing the footprint. This makes the technique much more suitable for low-power resonant WPT systems such as those covered by the wireless power consortium's Qi standard. In this section, the trends observed in Fig. 10 are confirmed experimentally, then compared to

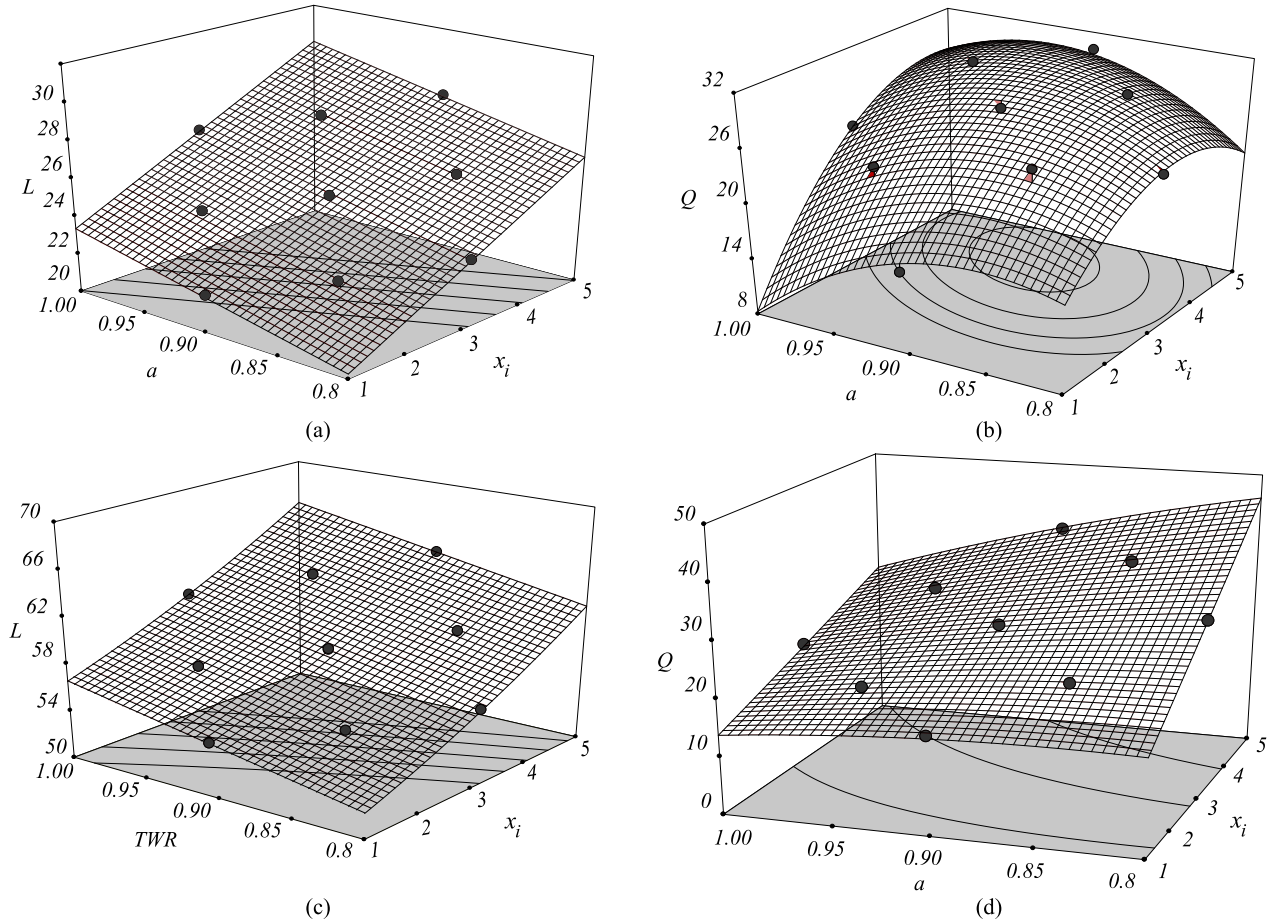

Fig. 10. 3-D representations of the inductance and quality factor for windings described in Table I at 200 kHz (a) inductance of two-layer windings in μH (b) quality factor of two-layer windings (c) inductance of four-layer windings in μH (d) quality factor of four layer windings.

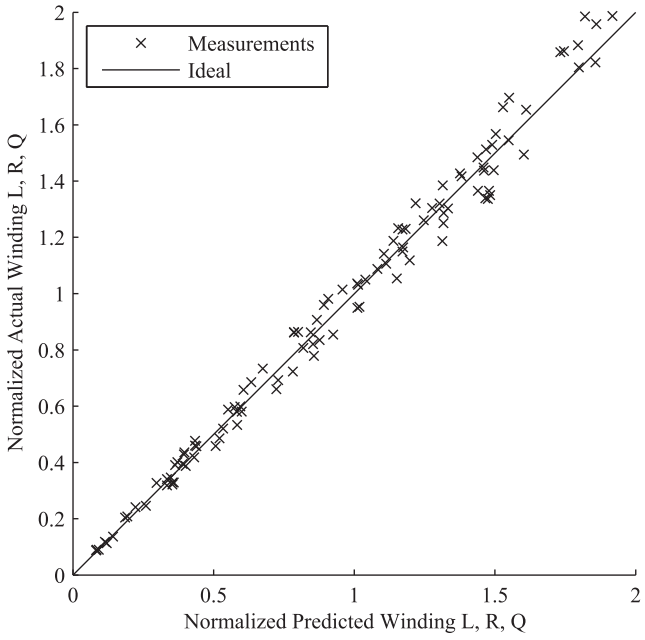

Fig. 11. Normalized actual versus predicted data for L, R, and Q for circular planar spiral windings employing a variety of turns, inner radius, and TWR. L is normalized to 40 μH, R was normalized to 250 $m\Omega$, and Q was normalized to 25.

experimental data from the approach of removing inner turns, and finally three windings are chosen for testing in a 5 W WPT system and their transmission efficiencies are documented: the baseline case, the best case winding with turns removed, and the best case proposed hollow planar spiral windings with TWR applied. The domain of the winding design is as defined in Table I, and the specifications of the WPT system are contained in Table II.

The maximum frequency of operation is 200 kHz, which is where the ac losses will be at their worst. This is the frequency the windings will be designed for. At 25 μH inductance, a two-layer solution is chosen due to inspection of Fig. 10, whose surface was used to define a locus of designs for which the inductance is predicted to stay at 25 μH. A series of spirals were manufactured to confirm this behavior, and were compared to the trends provided from Fig. 10. The results are presented in Fig. 12(c). The data points follow 25 μH inductance line and plot the resistance and Q of the combination, up to the point calculated here as the maximum. The inductance stays approximately constant, while the resistance decreases greatly, culminating in a Q which is over twice the initial value. These results are then compared with those achieved from hollowing the planar spiral by removing inner turns. In this case, the procedure was straightforward: measure L, R, and Q of a series of spirals in which one turn is removed at a time and observe the results.

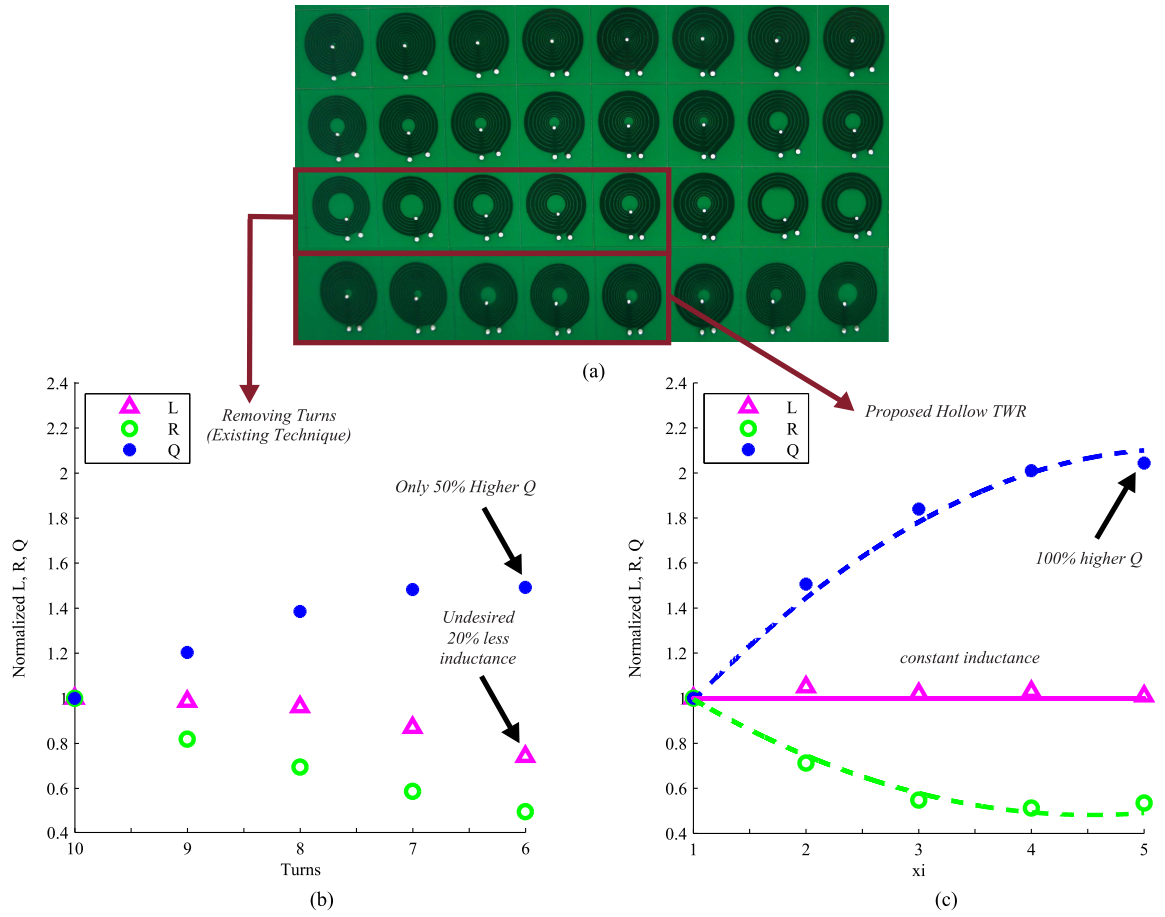

Fig. 12. (a) Subset of experimental windings employed to test the accuracy of the models. (b) Normalized representation of the performance of hollow planar spiral windings by removing turns. Q is normalized to 15, L is normalized to 25 μH, and R is normalized to 475 $m\Omega$. A 15% reduction in L is observed in order to attain a Q which is 50% higher. (c) Normalized experimental confirmation for L, R, and Q of two-layer proposed hollow circular planar spiral windings with TWR. Q is normalized to 15, L is normalized to 25 μH, and R is normalized to 475 $m\Omega$. It can be observed that by tuning the combination of x_i and a, the inductance stays almost constant while Q doubles.

TABLE II
WPT EXPERIMENTAL SPECIFICATIONS

Factor	Value	Units
L	25	μH
N_L	2	
f_r	100	kHz
f	105–200	kHz
l	10	mm
V_{in}	19	V
P_{out}	5	W

The data for this particular case is displayed in Fig. 12(b). The Q only reaches 50% higher than the baseline case, and at that point the inductance is reduced by 20%. This will also require a capacitor which is 25% larger in order to achieve the same resonant frequency for wireless power transmission. The proposed technique of increasing the internal radius and applying TWR has more flexibility and provides a nearly constant value of inductance. This is intuitive as the resistance decreases when the turns are shifted from the high field in the center, and the shorter turn lengths get matched with smaller winding widths. The inductance increases from the effect of hollowing, then decreases from the application of TWR, which provides the tunable inductance.

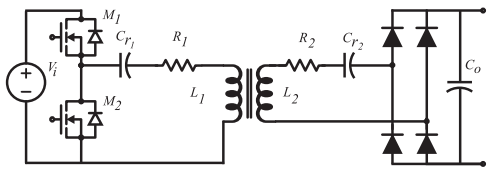

Fig. 13. Experimental WPT circuit setup.

Three windings were placed in a WPT system, whose simplified circuit diagram is included in Fig. 13: the completely filled winding (baseline), the highest-Q option when turns were removed, and the highest-Q option when the inner radius was increased and TWR was applied. The series capacitors were chosen in order for resonance to occur at 100 kHz, and operation was swept from 105 to 200 kHz. A deconstructed view of the proposed winding setup in the WPT transmission system is displayed in Fig. 14 with no alignment aids or connections such that the spiral can be observed.

Efficiency was compared at full load (5 W) condition. The best efficiency in each case was at around 170 kHz, in which the baseline case had a 70% transmission efficiency (see Fig. 15), the winding with turns removed had 80% (see Fig. 16), and the proposed winding had 90% (see Fig. 17). As predicted by the modeling, the proposed design method pushes

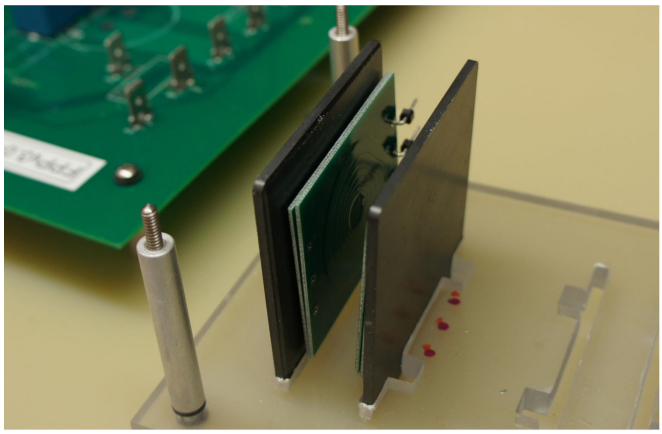

Fig. 14. WPT system with proposed hollow planar spiral windings with TWR. Several connections and alignment aids have been removed to add clarity.

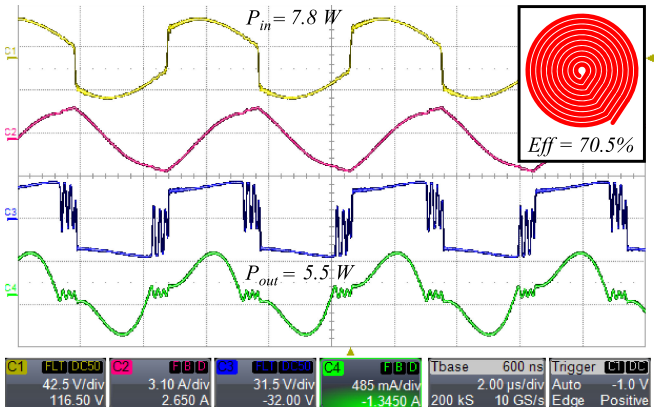

Fig. 15. Input voltage, input current, output voltage, and output current of the WPT system employing the baseline full planar spiral windings with a unity TWR at 170 kHz. Input power is 7.8 W and output power is 5.5 W, demonstrating a 70.5% efficiency.

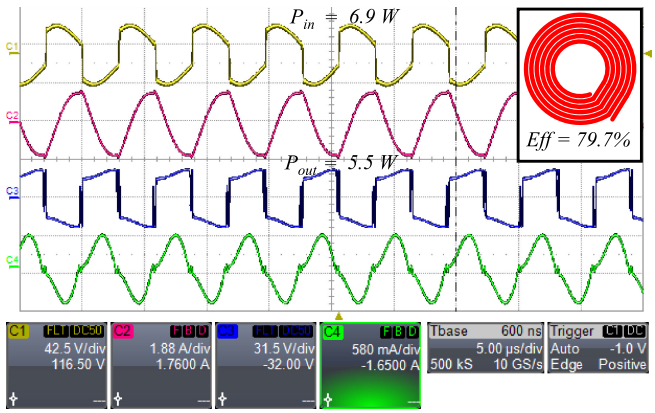

Fig. 16. Input voltage, input current, output voltage, and output current of the WPT system employing hollow planar spiral windings with four turns removed at 170 kHz. Input power is 6.9 W and output power is 5.5 W, demonstrating a 79.7% efficiency.

planar spiral windings to exceptional efficiencies. The resulting low-profile, high-efficiency winding can be used for WPT in slim consumer electronics for battery charging purposes.

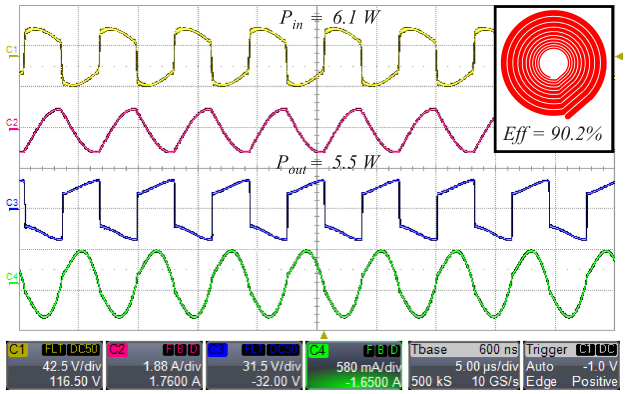

Fig. 17. Input voltage, input current, output voltage, and output current of the WPT system employing the proposed hollow planar spiral windings with nonunity TWR at 170 kHz. Input power is 6.1 W and output power is 5.5 W, demonstrating a 90.2% efficiency, the highest performance of the experimental cases.

VI. Conclusion

This study introduced the hollow spiral winding with TWR as a means of improving the quality factor of WPT systems. Models for the inductance were derived from the fundamentals provided by Grover and Greenhouse while the ac resistance models were derived from the most recent literature on ac power losses in planar spiral windings. The resultant behavior demonstrated a capability to design spiral windings with a tunable inductance and maximum quality factor. An experimental design case proved the superiority of the technique, with a doubling of the quality factor of the winding was observed. When the efficiency of power transfer was measured, a considerable jump was demonstrated, from 70% transfer efficiency for the full winding to 90% using the proposed method in a 5-W, 110–200-kHz WPT system based on the wireless power consortium Qi standard.

References

[1] B. Choi, J. Nho, H. Cha, T. Ahn, and S. Choi, "Design and implementation of low-profile contactless battery charger using planar printed circuit board windings as energy transfer device," *IEEE Trans. Ind. Electron.*, vol. 51, no. 1, pp. 140–147, Feb. 2004.

[2] P. Meyer, P. Germano, M. Markovic, and Y. Perriard, "Design of a contactless energy-transfer system for desktop peripherals," *IEEE Trans. Ind. Appl.*, vol. 47, no. 4, pp. 1643–1651, Jul. 2011.

[3] H. Matsumoto, Y. Neba, K. Ishizaka, and R. Itoh, "Model for a three-phase contactless power transfer system," *IEEE Trans. Power Electron.*, vol. 26, no. 9, pp. 2676–2687, Sep. 2011.

[4] H. Matsumoto, Y. Neba, and K. Ishizaka, "Comparison of characteristics on planar contactless power transfer systems," *IEEE Trans. Power Electron.*, vol. 27, no. 6, pp. 2980–2993, Jun. 2012.

[5] S. Raju, R. Wu, M. Chan, and C. P. Yue, "Modeling of mutual coupling between planar inductors in wireless power applications," *IEEE Trans. Power Electron.*, vol. 29, no. 1, pp. 481–490, Jan. 2014.

[6] J. Deng, W. Li, T. D. Nguyen, S. Li, and C. C. Mi, "Compact and efficient bipolar coupler for wireless power chargers: Design and analysis," *IEEE Trans. Power Electron.* vol. 30, no. 11, pp. 6130–6140, Nov. 2015.

[7] J. Sallán, J. Villa, A. Llombart, and J. F. Sanz, "Optimal design of ICPT systems applied to electric vehicle battery charge," *IEEE Trans. Ind. Electron.*, vol. 56, no. 6, pp. 2140–2149, Jun. 2009.

[8] D. Kürschner, C. Rathge, and U. Jumar, "Design methodology for high efficient inductive power transfer systems with high coil positioning flexibility," *IEEE Trans. Ind. Electron.*, Vol. 60, no. 1, pp. 372–381, Jan. 2013.

[9] D. Ahn and S. Hong, "A study on magnetic field repeater in wireless power transfer," *IEEE Trans. Ind. Electron.*, vol. 60, no. 1, pp. 360–371, Jan. 2013.

[10] W. Zhong, C. K. Lee, and S. Y. R. Hui, "General analysis on the use of Tesla's resonators in domino forms for wireless power transfer," *IEEE Trans. Ind. Electron.*, vol. 60, no. 4, pp. 261–270, Jan. 2013.
[11] D. Ahn and S. Hong, "Wireless power transmission with self-regulated output voltage for biomedical implant," *IEEE Trans. Ind. Electron.*, vol. 61, no. 5, pp. 2225–2235, May 2014.
[12] A. Zaheer, G. A. Covic, and D. Kacprzak, "Bipolar pad in a 10-kHz 300-W distributed IPT system for AGV applications," *IEEE Trans. Ind. Electron*, vol. 61, no. 7, pp. 3288–3301, Jul. 2014.
[13] S. Y. R. Hui, W. Zhong, and C. K. Lee, "A critical review of recent progress in mid-range wireless power transfer," *IEEE Trans. Power Electron.*, vol. 29, no. 9, pp. 4500–4511, Sep. 2014.
[14] J. Craninckx and M. S. J. Steyaert, "A 1.8 GHz low-phase-noise CMOS VCO using optimized hollow spiral inductors," *IEEE J. Solid-State Circuits*, vol. 32, no. 5, pp. 736–744, May 1997.
[15] Y. Su, X. Liu, C. K. Lee, and S. Y. R. Hui, "On the relationship of quality factor and hollow winding structure of coreless printed spiral winding (CPSW) inductor," *IEEE Trans. Power Electron.*, vol. 27, no. 6, pp. 3050–3056, Jun. 2012.
[16] X. Huang, K. D. T. Ngo, and G. Bloom, "Design techniques for planar windings with low resistance," in *Proc. 10th Annu. Appl. Power Electron. Conf. Expo.*, 1995, pp. 533–539.
[17] H. M. Hsu and C. W. Tseng, "Design of on-chip transformer with various coil widths to achieve minimal metal resistance," *IEEE Electron Device Lett.*, vol. 28, no. 11, pp. 1029–1032, Nov. 2007.
[18] S. R. Cove, M. Ordonez, F. Luchino, and J. E. Quaicoe, "Applying response surface methodology to small planar transformer winding design," *IEEE Trans. Ind. Electron.*, vol. 60, no. 2, pp. 483–493, Feb. 2013.
[19] H. M. Hsu, "Analytical formula for inductance of metal of various widths in spiral inductors," *IEEE Trans. Electron Devices*, vol. 51, no. 8, pp. 1343–1346, Aug. 2004.
[20] J. M. López-Villegas, J. Samitier, C. Cané, P. Losantos, and J. Bausells, "Improvement of the quality factor of RF integrated inductors by layout optimization," *IEEE Trans. Microw. Theory Tech.*, vol. 48, no. 1, pp. 76–83, Jan. 2000.
[21] P. L. Dowell, "Effects of eddy currents in transformer windings," *Proc. Inst. Electr. Eng.*, vol. 113, no. 8, pp. 1387–1394, Aug. 1966.
[22] N. H. Kutkut, "A simple technique to evaluate winding losses including two dimensional edge effects," in *Proc. IEEE Appl. Power Electron. Conf. Expo.*, Feb. 1997, pp. 368–374.
[23] T. Demeester and D. De Zutter, "Internal impedance of composite conductors with arbitrary cross section," *IEEE Trans. Electromagn. Compat.*, vol. 51, no. 1, pp. 101–107, Feb. 2009.
[24] I. Lope, C. Carretero, J. Acero, R. Alonso, and J. Burdio, "AC power losses model for planar windings with rectangular cross-sectional conductors," *IEEE Trans. Power Electron.*, vol. 29, no. 1, pp. 23–28, Jan. 2014.
[25] F. W. Grover, *Inductance Calculations*. Princeton, NJ, USA: Van Nostrand, 1946; reprinted New York, NY, USA: Dover, 1962.
[26] H. M. Greenhouse, "Design of planar rectangular microelectronic inductors," *IEEE Trans. Parts, Hybrids, Packag. Technol.*, vol. 10, no. 2, pp. 101–109, Jun. 1974.
[27] Wireless Power Consortium, "System description: Wireless power transfer," vol. 1, part 1, pp. 139–247, Jun. 2013.

Samuel R. Cove (S'05–M'15) was born in St. Johns, NL, Canada. He received the B.Eng. and M.Eng. degrees in electrical engineering from Memorial University, St. Johns, NL, Canada, in 2009 and 2011, respectively. He is currently working toward the Ph.D. degree at The University of British Columbia, Vancouver, BC, Canada.

His research interests include planar magnetics with applications in wireless power transfer, high-frequency resonant power conversion, and soft-switching power conversion topologies for renewable energy applications.

Mr. Cove received numerous prestigious scholarships and awards, including the UBC Four Year Fellowship (2014), the Natural Sciences and Engineering Research Council Postgraduate and Canadian Graduate Scholarships (2011 and 2010), the CD Nelson Memorial Scholarship (2011), and the Deans Excellency Award (2010). He was a Fellow of the School of Graduate Studies (2011), Memorial University of Newfoundland, for his academic excellence and involvement in the student community.

Martin Ordonez (S'02–M'09) was born in Neuquen, Argentina. He received the Ing. degree in electronics engineering from the National Technological University, Cordoba, Argentina, in 2003, and the M.Eng. and Ph.D. degrees in electrical engineering from the Memorial University of Newfoundland (MUN), St. Johns, NL, Canada, in 2006 and 2009, respectively.

He is currently the Canada Research Chair in Power Converters for Renewable Energy Systems and an Assistant Professor with the Department of Electrical and Computer Engineering, University of British Columbia, Vancouver, BC, Canada. He was an Adjunct Professor with Simon Fraser University, Burnaby, BC, Canada, and MUN. His industrial experience in power conversion includes research and development at Xantrex Technology Inc./Elgar Electronics Corp. (now AMETEK Programmable Power in San Diego, CA, USA), Deep-Ing Electronica de Potencia (Rosario, Argentina), and TRV Dispositivos (Cordoba, Argentina). With the support of industrial funds and the Natural Sciences and Engineering Research Council, he has contributed to more than 90 publications and R&D reports.

Dr. Ordonez is an Associate Editor of the IEEE TRANSACTIONS ON POWER ELECTRONICS, serves on several IEEE committees, and reviews widely for IEEE/IET journals and international conferences. He received the David Dunsiger Award for Excellence in the Faculty of Engineering and Applied Science (2009) and the Chancellors Graduate Award/Birks Graduate Medal (2006), and became a Fellow of the School of Graduate Studies, MUN.

Navid Shafiei (S'11) received the B.S degree in electrical engineering from Kashan University, Kashan, Iran, in 2005, and the M.S degree in electrical engineering from Islamic Azad University, NajafAbad branch, Iran, in 2011. He is currently working toward the Ph.D. degree at The University of British Columbia in Vancouver, BC, Canada.

He was a Technical Designer in the Information and Communication Technology Institute at Isfahan University of Technology, Iran, from 2005 to 2013, where he was involved in design and implementation of resonant converters. His current research interests include resonant converters and their application in pure electric vehicles.

Jianglin Zhu (S'14) received the B.E. degree in electrical engineering from the Huazhong University of Science and Technology, Wuhan, China, in 2015. He is currently working toward the Ph.D. degree in the University of Colorado at Boulder, CO, USA.

His research interests include high-efficiency electric vehicle power electronics with WBG devices, integrated magnetics, and wireless power transfer.